# SELF-SIMILAR FOLD EVOLUTION UNDER PRESCRIBED END-SHORTENING

CHRIS J. BUDD, GILES W. HUNT, AND MARK A. PELETIER

Abstract. The evolution of single-layer folds under prescribed end-shortening conditions displays folds of varying wavelength. We investigate a simple model of this kind and characterize the long-term behaviour of fold profiles. In particular we determine the evolution of the axial load and the variation of the wavelength, and we show that the fold profiles are highly self-similar.

## 1. Introduction

The variety of folding patterns in geological strata has always inspired a particular fascination. It seems intuitively obvious that some mechanism should be responsible for the selection between the different observed forms; but although many models and mechanisms have been proposed, there is a widespread feeling that the process of folding is still not well understood. For more than fifty years analytical models have been proposed as a means of understanding folding. Single-layer folding models mostly take the form of a thin layer embedded in a homogeneous matrix subject to compression parallel to the layer.

The creation—and subsequent deformation—of a fold necessarily spans a certain time, and that it therefore is natural to think of the process as an *evolution* from the straight layer (probably with perturbations) via creation, amplification, and finally freezing to the form that is eventually observed. From this perspective it is interesting to note that many of the more traditional models—notably the 'dominant wavelength' family—retain only a caricature of this evolution in the form of a comparison of different growth rates. There is clearly much to be gained from a faithful modelling of the complete evolution process.

In the modelling of folding as an evolution process one issue in particular has a marked influence on the response. The traditional formulation considers fold evolution under a prescribed layer-parallel load. In recent years, however, it has become clear that fold evolution under prescribed end-shortening (or total strain) may be more realistic (Mühlhaus, Hobbs and Ord, 1994; Hunt, Mühlhaus and Whiting, 1996; Whiting, 1996; Whiting and Hunt, 1997). The purpose of this paper is to analyse and extend simple models of this kind, place the results on a mathematical footing, and generally provide new insights. Where appropriate, numerical results are used to illustrate these. Notably our findings of (approximate) self-similarity in models of single-layer folding seem to be new.

We model single-layer folding by an unbounded elastic layer embedded in a viscous matrix (see Figure 1). The constitutional laws are linear, and small deflections

*Date*: June 1, 1998.

*Key words and phrases.* long-term asymptotics, fold characterization, variable wavelength, viscous winkler foundation, viscous halfspace.

The authors are grateful to the EPSRC for their funding of this project through grant GR/L17177 of the Applied Nonlinear Mathematics Initiative.

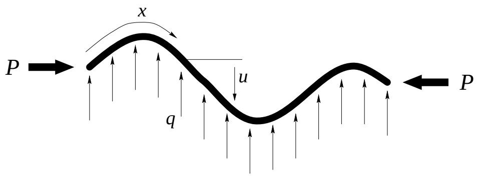


FIGURE 1. An elastic layer on a viscous bedding

are assumed. The equations governing this model are (after rescaling)

$$u_t + u_{xxxx} + Pu_{xx} = 0 \qquad -\infty < x < \infty \tag{1}$$

$$\frac{1}{2}\int_{-\infty}^{\infty} u_x^2\,dx = g(t). \tag{2}$$

The first equation is a force balance, where $u = u(x,t)$ is the vertical displacement of the layer, $x$ the horizontal distance measured along the layer, $P = P(t)$ the axial (layer-parallel) load, and $u_x$ is assumed small. Subscripts denote differentiation. Equation (2) describes the condition of prescribed end-shortening. The function $g(t)$ is given; with tectonic compression in mind a typical function $g(t)$ might be $a + bt$. Note that prescribing the end-shortening implies that $P$ is free and needs to be determined as part of the solution (see Section 2 for the details of the derivation of these equations). We show that for all localized initial data this equation has a unique, localized, globally attracting self-similar behaviour.

The equation for the layer itself is completely linear; the only nonlinearity in the problem is the constraint (2). However, this constraint has profound effects on the behaviour of the model. We mention a number of these effects below.

*1. Localized folds remain localized.* A consequence of the evolutionary aspect of the model is that a localized initial perturbation gives rise to a localized subsequent fold evolution. Figure 2 shows an example of how an initial perturbation evolves[1] for a linearly increasing end-shortening function $g$.

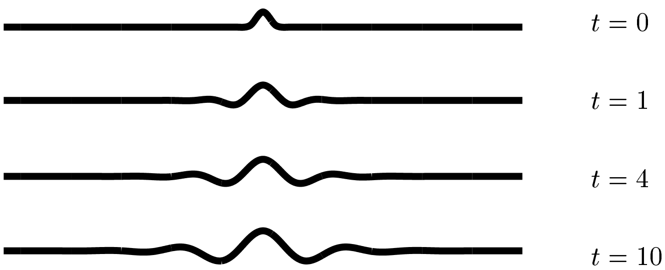


FIGURE 2. Evolution of the deformed layer

The unboundedness of the layer has nothing to do with this property: long but finite layers should evolve in a similar way to unbounded layers, provided the perturbation itself is localized, and up to the time when the folds reach the ends

[1] The example profiles shown in this paper are calculated using a finite-element discretization in space, based on Hermite cubic polynomials. Since equation (2) contains no time derivative, the resulting problem is a differential-algebraic equation. This equation was solved with the differential-algebraic equation solver DDASSL (Petzold, 1982). See the companion paper Budd and Peletier (1998) for the details of this calculation.

of the layer. In a similar vein, two localized perturbations far apart should evolve independently until the spreading of the folds makes them interfere with each other.

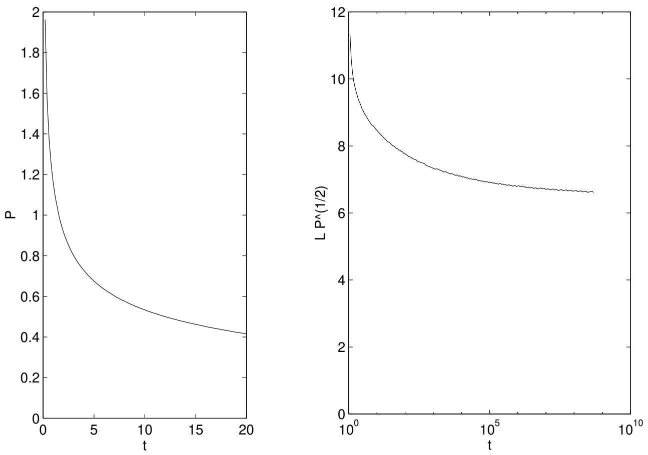


(a) Load *vs.* time

(b) Scaled wavelength $L\sqrt{P}$ *vs.* time

FIGURE 3. Evolution of load $P$ *vs.* time and scaled wavelength $L\sqrt{P}$ for a constant end-shortening evolution

*2. Wavelength and axial load change through time.* Whilst the profiles of Figure 2 remain localized, there is a clear increase in wavelength as time increases. This is coupled to a marked decrease in $P$ (Figure 3(a)).

The case of constant load in this model set-up (small deflections, an elastic layer on a viscous foundation) was studied first by Biot (1965). He found a relationship between $P$ and the wavelength $L$ of the type

$$L = \frac{c}{\sqrt{P}}$$

where $c$ is a constant depending on the layer thickness and the elastic parameters of the layer (in the case of equation (1), where coefficients have been rescaled, $c = 2\pi$). Figure 3(b) shows the product $L\sqrt{P}$ for a long-term calculation. While there is a clear discrepancy initially, for large times $L\sqrt{P}$ approaches the value $2\pi$, independent of initial conditions. This effect is simply explained: as time advances, $P$ varies less rapidly, and Biot's approximation by a constant load gains in accuracy. Note however the time scale on which this convergence takes place.

This variation in wavelength demonstrates an important property of prescribed end-shortening models (see also Mühlhaus et al., 1994; Whiting and Hunt, 1997; Whiting, 1996): *there is no dominant wavelength* valid over all timescales.

*3. The long-term evolution is self-similar.* As shown in Figure 4(a) the calculated profiles show a simultaneous increase in amplitude and in wavelength as time advances. Under a suitable rescaling, however—see Figure 5—the differences are strongly reduced. In the analysis in Section 4 we determine the exact asymptotic behaviour in the limit $t \to \infty$. For instance, in the case of constant end-shortening ($g(t) = a > 0$) we have

$$u(x,t) \sim A\sqrt{a}\,\frac{t^{1/8}}{[\log t]^{1/4}}\,e^{-y^2/6\log t}\cos y \tag{3}$$

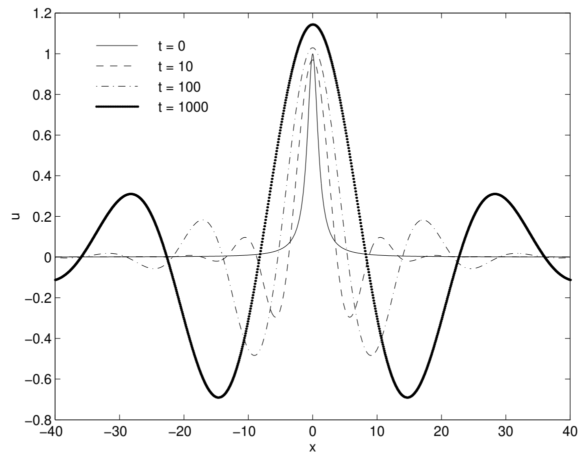


(a) Initial data $1/(1+x^2)$

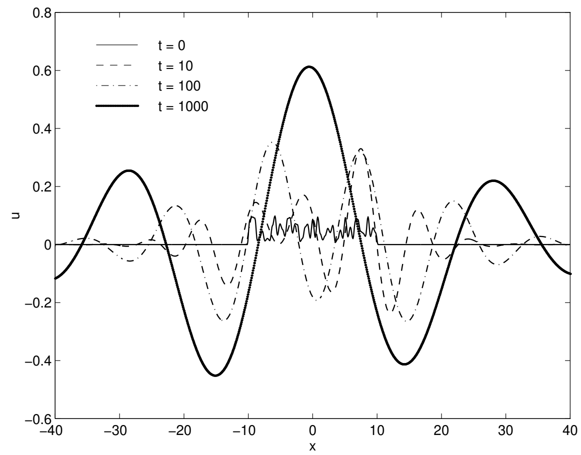


(b) Random initial data on the interval $[-10, 10]$ with maximum 0.1

FIGURE 4. Evolution of the solution profile $u$ under constant end-shortening.

where $y = Bxt^{-1/4}[\log t]^{1/4}$ and $A$ and $B$ are constants. Figure 6 shows a numerically calculated solution compared to the asymptotic profile (3). Note that on most time scales $\log t$ can be considered constant in comparison to powers of $t$, reducing (3) to

$$u(x,t) \sim \tilde{A}\sqrt{a}\, t^{1/8}\, e^{-cy^2} \cos y \tag{4}$$

with $y = \tilde{B}xt^{-1/4}$ for slowly varying functions $\tilde{A}$, $\tilde{B}$, and $c$.

This formula shows that profiles are self-similar in the long term: at different times the profiles have the same form, but rescaled ('vertically' by a factor $t^{1/8}$, and 'horizontally' by a factor $t^{1/4}$). Again we see in this long-term behaviour that the wavelength continues to increase and tends to infinity in the limit $t \to \infty$.

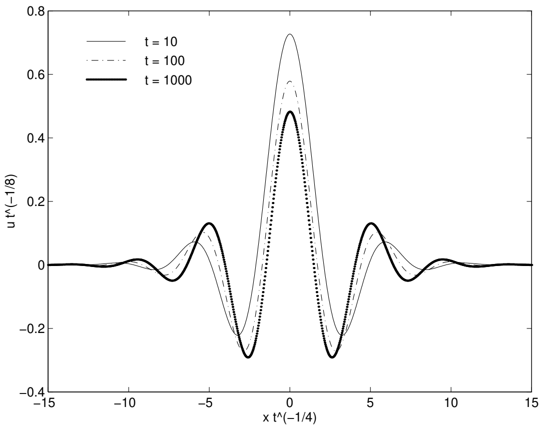


FIGURE 5. The same evolution as Figure 4(a), but presented in self-similar variables. In these variables an exact self-similar solution would appear constant.

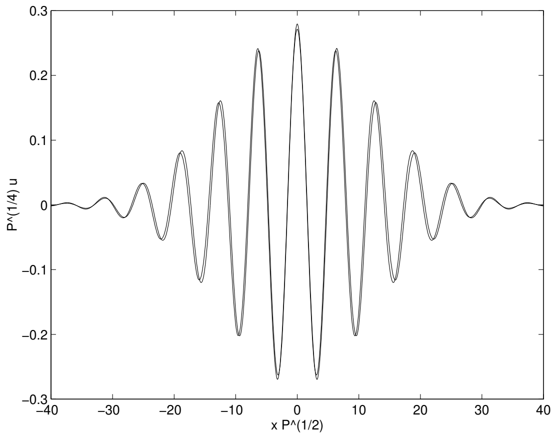


FIGURE 6. Comparison between the numerically calculated solution and the asymptotic profile (constant end-shortening). The scales have been chosen in accordance with (14).

*4. Independence of initial perturbations.* An important consequence of (3), one which merits separate mention, is that the long-term behaviour has a generic form and is therefore independent of the form of the initial perturbation.

There are a number of results in the literature that focus on the relationship between the shape of the initial perturbation and that of the subsequent folds (Cobbold, 1975; Cobbold, 1977; Williams, Lewis and Zienkiewicz, 1978; Abbasi and Mancktelow, 1990; Abbasi and Mancktelow, 1992; Mancktelow and Abbasi, 1992; Zhang, Hobbs, Ord and Mühlhaus, 1996). The independence of initial data mentioned above does not contradict these findings, but merely indicates that the correspondence between initial form and subsequent folds weakens as the folds evolve.

This is illustrated by Figures 4(a) and 4(b). The initial stages of fold development are clearly different in the two cases, but at larger times there is a strong similarity.

Note that although the early stages of fold development in Figure 4(b) do not resemble the generic fold shape that appears in the later stages, the increase in wavelength can be observed almost immediately.

*5. The importance of (geometric) large-deflection effects may be either small or large, depending on the end-shortening function $g(t)$.* The derivation of (1-2) involves the assumption that the limb angle is small. As mentioned above, the large-time behaviour under *constant* end-shortening is (roughly) of the form

$$u(x,t) \sim t^{1/8} f(xt^{-1/4}). \tag{5}$$

The limb angle is related to the derivative $u_x$ which will have a long-term form

$$u_x(x,t) \sim t^{-1/8} f'(xt^{-1/4})$$

by the chain rule. Consequently the maximum of $|u_x|$ over $x \in \mathbb{R}$ is equal to

$$t^{-1/8} \max_{y\in\mathbb{R}} |f'(y)|$$

and therefore tends to zero as $t \to \infty$. Hence the assumption that $u_x$ is small becomes increasingly accurate in the long-term limit. We expect therefore that a geometrically nonlinear model will share the same long-term behaviour.

The situation is different for a linearly increasing end-shortening. Here the long-term behaviour takes the form

$$u(x,t) \sim t^{5/8} f(xt^{-1/4})$$

so that

$$u_x(x,t) \sim t^{3/8} f'(xt^{-1/4}),$$

implying that the maximum limb angle *grows* in time. Consequently the small-deflection approximation becomes less accurate in time, and we expect the two to differ strongly in the limit $t \to \infty$.

The rest of this paper is structured as follows. In Section 2 we derive the model. In Section 3 we discuss self-similar solutions, and the full long-term behaviour of the solutions is derived in Section 4. Our techniques are heavily based on the use of the continuous Fourier transform on the real line, and in the Appendix we state a number of properties of this transform. Most of the details of proofs have been left out. The interested reader can find a rigorous treatment of these results in Budd and Peletier, 1998.

## 2. The Model

We consider a thin linear elastic layer on a linear viscous bedding, as in Figure 1. Assuming small deflections, the equation for the vertical deflection $u$ is

$$Du_{xxxx} + Pu_{xx} + q = 0 \qquad -\infty < x < \infty,\ t > 0, \tag{6}$$

where $q$ is the bedding force and $P = P(t)$ the axial load on the elastic layer, and $x$ is the distance along the layer (arc length). The bending stiffness $D$ is equal to $Eh^3/12(1-\nu^2)$, where $h$ is the thickness of the layer. Note that we consider this equation on the whole real line.

We consider two types of foundation: (a) a linear viscous Winkler foundation, and (b) a linear viscous halfspace. For the Winkler foundation the force $q$ is simply given by $q = \eta u_t$ ($\eta$ is the viscosity); for the halfspace $q = 4\eta H(u_{xt})$ (Biot, 1965, p. 419), where $H$ is the Hilbert transform (see Appendix A for the definition of the Fourier and Hilbert transforms). By rescaling the various coefficients this leads to

$$\text{(Winkler foundation)} \qquad u_t + u_{xxxx} + Pu_{xx} = 0 \tag{7}$$

and

$$\text{(halfspace)} \qquad H(u_{xt}) + u_{xxxx} + Pu_{xx} = 0. \tag{8}$$

The reasons for considering two different foundations are twofold. First, the Winkler foundation is simpler in concept and implementation, while the viscous halfspace is closer to reality. Secondly, the fact that the long-term results are similar in nature for the two foundations indicates that only the viscous quality of the foundation is of importance for the long-term behaviour; other properties play a minor role.

As mentioned above, $P$ is not prescribed; instead the total end-shortening is supposed to be equal to a given function of time. By using a small-deflection approximation, this can be modelled as

$$\frac{1}{2}\int_{-\infty}^{\infty} u_x^2(x)\,dx = g(t) \qquad t \geq 0. \tag{9}$$

Here the function $g(t)$ is the prescribed amount of end-shortening. If we supplement these equations with an initial condition

$$u(x,0) = u_0(x) \qquad -\infty < x < \infty, \tag{10}$$

and assume that $u_0$ satisfies (9)—i.e., $\int u_{0x}^2 = g(0)$—then this problem has a unique solution $(u, P)$. Note that $u$ is a function of $x$ and $t$, but $P$ is a function of time only.

## 3. Large-time behaviour I: Self-similar solutions

We can make an educated guess of the large-time behaviour of solutions by considering the scaling invariance of the equations. Taking as an example the Winkler foundation model with a constant end-shortening (constant $g(t)$), equation (7) is invariant under the scaling

$$x \to \lambda^{1/4}x, \quad t \to \lambda t, \quad P \to \lambda^{-1/2}P,$$

and so we might expect to find self-similar solutions that scale accordingly, i.e. solutions of the form

$$u(x,t) = t^{1/8}f(xt^{-1/4}), \qquad P(t) = Qt^{-1/2}. \tag{11}$$

The factor $t^{1/8}$ is chosen as to satisfy the constraint:

$$\begin{aligned}\int u_x^2(x,t)\,dx &= \int (t^{-1/8}f'(xt^{-1/4}))^2\,dx \\ &= \int f'(xt^{-1/4})^2\,dxt^{-1/4} = \int f'(\xi)^2\,d\xi,\end{aligned}$$

where the primes denote differentiation with respect to the self-similar variable $\xi = xt^{-1/4}$. If a function $u$ of the form (11) satisfies equation (7), then the profile $f$ solves the ordinary differential equation

$$f'''' + Qf'' + \frac{1}{8}f - \frac{1}{4}\xi f' = 0 \qquad -\infty < \xi < \infty, \tag{12}$$

and the constraint

$$\frac{1}{2}\int f'(\xi)^2\,d\xi = g \quad \text{(constant)}. \tag{13}$$

However, the system of equations (12-13) has no solutions. This can be seen from translating the equation to the Fourier domain. Applying the Fourier transform to equation (12) we find, writing $\hat{f}$ for $\hat{f}(\omega)$,

$$\omega^4\hat{f} - Q\omega^2\hat{f} + \frac{1}{8}\hat{f} - \frac{1}{4\sqrt{2\pi}}\hat{\xi} * (i\omega\hat{f}) = 0.$$

Using $\hat{\xi} = i\sqrt{2\pi}\,\delta'$, where $\delta$ is the Dirac delta function,

$$\begin{aligned}\left[\hat{\xi} * (i\omega\hat{f})\right](\omega) &= -\sqrt{2\pi}\,\delta' * (\omega\hat{f}) \\ &= -\sqrt{2\pi}\,\delta * (\omega\hat{f})' \\ &= -\sqrt{2\pi}\,(\omega\hat{f})' \\ &= -\sqrt{2\pi}(\hat{f} + \omega\hat{f}').\end{aligned}$$

Here $\hat{f}'(\omega) = d/d\omega\,\hat{f}(\omega)$. We find that $\hat{f}$ satisfies

$$\hat{f}\left(\omega^4 - Q\omega^2 + \frac{3}{8}\right) + \frac{1}{4}\omega\hat{f}' = 0,$$

which can also be written as

$$\frac{\hat{f}'}{\hat{f}} = -\frac{3}{2}\omega^{-1} - 4\omega^3 + 4Q\omega.$$

Close to $\omega = 0$ the behaviour of $\hat{f}$ is given by the first term on the right-hand side, so that if $f$ is non-zero, then

$$\hat{f}(\omega) \sim |\omega|^{-3/2} \qquad \text{as } \omega \to 0.$$

Hence

$$\int f'(\xi)^2\,d\xi = \int \omega^2 \left|\hat{f}(\omega)\right|^2 d\omega = \infty,$$

implying that $f$ can not satisfy condition (13). Hence there are no self-similar solutions of the exact form (11).

The non-existence of exact self-similar solutions implies that solutions can not have a long-term behaviour of self-similar form. However, the underlying scaling properties of the problem continue to drive the evolution along the lines of self-similarity. The result is a long-term behaviour that is *approximately self-similar*.

## 4. Large-time behaviour II: Approximate self-similarity

The actual large-time behaviour follows the self-similar scaling closely with a small (logarithmic) correction. We will discuss this now in some detail. For the precise statement of our result, and to combine several types of constraint functions $g$, we set

$$g(t) = a + bt^\gamma, \qquad a, \gamma \geq 0,\, b > 0.$$

The notation $\alpha \sim \beta$ denotes $\alpha/\beta \to 1$ as $t \to \infty$.

**Theorem 1** (Winkler foundation)**.** *Let $u$ be the solution of equations (7), (9) with initial datum $u_0$. As $t \to \infty$,*

$$P(t) \sim 2^{-1/2}\,t^{-1/2}[(\gamma + 3/4)\log t]^{1/2}$$

*and if*

$$u(x,t) = P^{-1/4}g^{1/2}v(xP^{1/2}, t) \tag{14}$$

*then*

$$v(y,t) \sim \sqrt{2}\,[\pi(\gamma + 3/4)\log t]^{-1/4} e^{-y^2/8(\gamma+3/4)\log t} \cos y. \tag{15}$$

**Theorem 2** (Halfspace)**.** *Let $u$ be the solution of equations (8), (9) with initial datum $u_0$. As $t \to \infty$,*

$$P(t) \sim 2^{-4/3}\, t^{-2/3}\, [(\gamma + 3/4)\log t]^{1/2}$$

*and if $u(x,t) = P^{-1/4} g^{1/2} v(xP^{1/2}, t)$, then*

$$v(y,t) \sim 2^{3/4}[3\pi(1+\gamma)\log t]^{-1/4} e^{-y^2/3(1+\gamma)\log t} \cos y.$$

**Remark 1** Depending on the time scales involved, the expressions above might be simplified by considering the logarithms in these expressions as slowly varying with respect to the powers of $t$. If so, then we find on combining (14) and (15) that for the Winkler foundation the fold profiles take the asymptotic form

$$u(x,t) \sim A\sqrt{b}\, t^{1/8+\gamma/2} e^{-cy^2} \cos y$$

where $y = Bxt^{-1/4}$, for some slowly varying functions $A, B, c > 0$. Similarly, the halfspace profiles take the form

$$u(x,t) \sim A\sqrt{b}\, t^{1/6+\gamma/2} e^{-cy^2} \cos y$$

where now $y = Bxt^{-1/3}$.

## 5. Analysis of the Winkler and halfspace models

In this section we give an intuitive derivation of Theorems 1 and 2. For a rigorous presentation we refer to the companion paper (Budd and Peletier, 1998). We will use the Winkler foundation case as an example; the halfspace case follows along the same lines.

Applying the Fourier transform in $x$, we transform equation (7) into an equivalent equation in $\omega$ (the Fourier variable) and $t$:

$$\hat{u}_t(\omega,t) + (\omega^4 - P(t)\omega^2)\hat{u}(\omega,t) = 0, \qquad -\infty < \omega < \infty,\ t > 0$$

where $\hat{u}$ is the Fourier transform of $u$. For a *given* function $P(t)$ and an initial datum $u_0(x)$ (or $\hat{u}_0(\omega)$) this equation can be solved explicitly:

$$\hat{u}(\omega,t) = \hat{u}_0(\omega) e^{-\omega^4 t + \Pi(t)\omega^2}, \tag{16}$$

where $\Pi(t) = \int_0^t P(\tau)d\tau$. Using the the fact that the Fourier transform conserves norms,

$$\int u_x(x,t)^2\, dx = \int |i\omega\hat{u}(\omega,t)|^2\, d\omega = \int \omega^2 |\hat{u}(\omega,t)|^2\, d\omega,$$

and we find on substitution of (16) that the end-shortening constraint (9) reads

$$\frac{1}{2}\int |\hat{u}_0(\omega)|^2 \omega^2 e^{-2\omega^4 t + 2\Pi(t)\omega^2}\, d\omega = g(t). \tag{17}$$

Solving problem (7), (9), (10) is therefore equivalent to finding a function $\Pi : [0,\infty) \to \mathbb{R}$ such that equation (17) holds for all $t > 0$. In (Budd and Peletier, 1998) we prove that such a function exists and is unique.

To investigate the behaviour of $\Pi$ for large $t$ we introduce the change of variables $\xi = \omega t^{1/4}$, $\Sigma(t) = t^{-1/2}\Pi(t)$, so that

$$\frac{1}{2}\int \left|\hat{u}_0(\xi t^{-1/4})\right|^2 \xi^2 e^{-2\xi^4 + 2\Sigma(t)\xi^2} d\xi = t^{3/4} g(t) =: h(t).$$

We expect that $\Sigma(t) \to \infty$ as $t \to \infty$. Since then $\xi^2 e^{-2\xi^4+2\Sigma(t)\xi^2}$ localizes around $\xi = 0$, one can expect that only the value $\hat{u}_0(0)$ is important for large $t$. This leads to

$$\frac{1}{2}\int \xi^2 e^{-2\xi^4+2\Sigma(t)\xi^2} d\xi = |\hat{u}_0(0)|^{-2}\ h(t),$$

provided $\hat{u}_0(0) \neq 0$. If we define

$$F(y) = \int \xi^2 e^{-2\xi^4+2y\xi^2}\, d\xi,$$

then the function $\Sigma(t)$ satisfies

$$\Sigma(t) = F^{-1}\left(2\,|\hat{u}_0(0)|^{-2}\ h(t)\right),$$

and hence we only need to determine the behaviour of $F(y)$ for large $y$, in order to know the long-term behaviour of $\Sigma$ and consequently $\Pi$ and $P$. Watson's Lemma (Theorem 7.1 in Olver, 1974) gives an asymptotic expression for $F(y)$:

$$F(y) \sim \frac{1}{2}\sqrt{\pi y}\, e^{y^2/2} \quad \text{or} \quad F^{-1}(z) \sim \sqrt{2\log z},$$

both in the limit $y, z \to \infty$. Thus

$$\Sigma(t) \sim \sqrt{2\log h(t)},$$

and since $h(t) \sim c\, t^{\gamma+3/4}$ (with $c = b$ if $\gamma > 0$ and $c = a + b$ if $\gamma = 0$),

$$\Sigma(t) \sim \sqrt{2(\gamma + 3/4)\log t} \qquad \text{as } t \to \infty.$$

Transforming back we find that $\Pi(t) \sim \sqrt{2(\gamma + 3/4)t\log t}$ and

$$P(t) \sim \frac{1}{2}t^{-1/2}\sqrt{2(\gamma + 3/4)\log t} \qquad \text{as } t \to \infty.$$

This proves the first part of Theorem 1.

To determine the long-term profile we examine the Fourier spectrum of the solution (given by (16)),

$$\hat{u}(\omega, t) = \hat{u}_0(\omega)e^{-\omega^4 t+\Pi(t)\omega^2}.$$

The exponent $-\omega^4 t + \Pi(t)\omega^2$ has a maximum of $\Pi(t)^2/4t$ at the values $\omega = \pm\sqrt{\Pi(t)/2t}$. Since $\Pi \sim \sqrt{2(\gamma + 3/4)t\log t}$, this maximum tends to infinity as $t \to \infty$. Consequently the spectrum $\hat{u}$ is dominated by two large spikes at these values of $\omega$. The long-term behaviour (15) is obtained by characterizing these spikes in a convenient way.

By the scaling law (21) the Fourier transform of $v$ is given by

$$\hat{v}(\xi, t) = P^{3/4}g^{-1/2}\hat{u}(\xi P^{1/2}, t) = P^{3/4}g^{-1/2}\hat{u}_0(\xi P^{1/2})e^{-P^2 t\xi^4+\Pi P\xi^2},$$

where $\xi = \omega P^{1/2}$. From the expressions for $P$ and $\Pi$ above we have $\Pi P/P^2 t \sim 2$, so that

$$-P^2 t\xi^4 + P\Pi\xi^2 \sim -P^2 t(\xi^4 - 2\xi^2) \qquad \text{as } t \to \infty. \tag{18}$$

Here the effect of the transformation (14) can be clearly seen: where the maxima in the spectrum of $\hat{u}$ move towards the origin, in $\hat{v}$ they move toward a fixed position $\xi = \pm 1$. Since the important contribution in the Fourier spectrum comes from the region around these maxima, we simplify by replacing $\xi^4 - 2\xi^2$ by a parabola centered on the maximum and with similar curvature, i.e.

$$\xi^4 - 2\xi^2 \longrightarrow 4(\xi - 1)^2 - 1 \qquad \text{for } \xi > 0, \tag{19}$$

and

$$\xi^4 - 2\xi^2 \longrightarrow 4(\xi + 1)^2 - 1 \qquad \text{for } \xi < 0. \tag{20}$$

To summarize, we claim that $\hat{v}$ converges to

$$\hat{z}(\xi,t) = \alpha(t)\left\{e^{-\beta(t)[4(\xi-1)^2-1]} + e^{-\beta(t)[4(\xi+1)^2-1]}\right\},$$

provided $\alpha$ and $\beta$ are chosen appropriately. It turns out (see Budd and Peletier, 1998 for the details) that

$$\beta \sim \frac{1}{2}(\gamma + 3/4)\log t \qquad \text{and} \qquad \alpha \sim \hat{u}_0(0)P^{3/4}g^{-1/2},$$

and these values lead to the result (15). Note that the asymptotic behaviour of $\beta$ coincides exactly with that of $P^2t$, as is to be expected from (18) and (19-20).

## 6. Conclusion

We have developed a new model for localized folds in an elastic layer embedded in a viscous matrix. This model takes into account the viscous aspects of the evolution and an end-shortening constraint. Localized folds remain localized, but widen through evolution, and show a continuously increasing wavelength. In addition we have completely characterized the long-term behaviour of these folds and the associated axial load.

This long-term behaviour is expected to apply not only to the viscous foundation of this model, but also to foundations that are visco-elastic, and also, in some cases, to geometrically nonlinear models (as explained in the Introduction). However, a long-term result begs the question of the short-term character of the model, and we hope to explore this question in the future. It should be noted that here the material properties are not irrelevant, and the difference between a visco-elastic and a viscous foundation should be visible.

A different extension, one that is hinted at in recent geological literature (Mühlhaus, Sakaguchi and Hobbs, n.d.), would be to consider not only the foundation but also the layer to be visco-elastic. This would change the large-time behaviour in a fundamental way, since the strain energy contained in the deformed layer can then dissipate viscously both in the foundation and in the layer. The ratio between the two viscosities is expected to be of prime importance in such a model.

Again a different, but equally interesting extension would consist in relaxing the small-deflection hypothesis, resulting in a geometrically nonlinear model for the layer. Numerical results by Whiting and Hunt (Whiting and Hunt, 1997) show interesting behaviour, especially for a relatively rapid increase in end-shortening. Here again, elastic properties could be significant.

## Appendix A. Fourier Analysis and the Hilbert Transform

The Fourier transform of a function $u : \mathbb{R} \to \mathbb{R}$ is defined by

$$\mathcal{F}(u)(\omega) = \frac{1}{\sqrt{2\pi}}\int u(x)e^{-i\omega x}\,dx.$$

We also write $\hat{u}(\omega)$ for $\mathcal{F}(u)(\omega)$. The inverse transform is

$$\mathcal{F}^{-1}(v)(x) = \check{v}(x) = \frac{1}{\sqrt{2\pi}}\int v(\omega)e^{i\omega x}\,d\omega,$$

This transform conserves $L^2$-norms identically, that is

$$\int |u(x)|^2\,dx = \int |\hat{u}(\omega)|^2\,d\omega,$$

and derivatives transform into polynomials:

$$\widehat{u'}(\omega) = i\omega\hat{u}(\omega).$$

The convolution product of two functions $f$ and $g$ on $\mathbb{R}$ is defined by

$$(f * g)(x) = \int_{\mathbb{R}} f(y)g(x-y)\,dy.$$

This product is symmetric in $f$ and $g$, has the property

$$(f * g)' = f' * g = f * g',$$

and interacts with Fourier transforms in a simple way:

$$\widehat{uv}(\omega) = \frac{1}{\sqrt{2\pi}}\,(\hat{u} * \hat{v})(\omega).$$

For convenience we also mention the scaling law

$$\widehat{u(\lambda x)}(\omega) = \frac{1}{\lambda}\hat{u}(\omega/\lambda). \tag{21}$$

The Hilbert Transform of a function $u : \mathbb{R} \to \mathbb{R}$ is defined as

$$H(u)(x) = \frac{1}{\pi}\int_{-\infty}^{\infty} \frac{u(y)}{x-y}\,dy,$$

where the integral should be taken as a principal value. There exists an elegant alternative formulation of the Hilbert Transform in terms of Fourier Transforms:

$$\widehat{H(u)}(\omega) = -i\,\mathrm{sgn}(\omega)\hat{u}(\omega).$$

## References


Abbasi, M. R. and Mancktelow, N. S. (1990). The effect of initial perturbation shape and symmetry on fold development, *J. Struct. Geol.* **12**(2): 273–282.

Abbasi, M. R. and Mancktelow, N. S. (1992). Single layer buckle folding in non-linear materials—i. experimental study of fold development from an isolated initial perturbation, *J. Struct. Geol.* **14**: 85–104.

Biot, M. A. (1965). *Mechanics of Incremental Deformations*, Wiley, New York.

Budd, C. J. and Peletier, M. A. (1998). Approximate self-similarity in models of geological folding, *Technical Report 98/09*, University of Bath.
**URL:** *http://www.maths.bath.ac.uk/Maths_Group/preprints.html*

Cobbold, P. R. (1975). Fold propatation in single embedded layers, *Tectonophysics* **27**: 333–351.

Cobbold, P. R. (1977). Finite-element analysis of fold propagation—a problematic application?, *Tectonophysics* **38**: 339–353.

Mühlhaus, H.-B., Sakaguchi, H. and Hobbs, B. E. (n.d.). Evolution of 3d folds for a non-newtonian plate in a viscous medium, *Proc. R. Soc. Lond.* . To appear.

Hunt, G. W., Mühlhaus, H.-B. and Whiting, A. I. M. (1996). Evolution of localized folding for a thin elastic layer in a softening visco-elastic medium, *Pure Appl. Geophys.* **146**: 229–252.

Mancktelow, N. S. and Abbasi, M. R. (1992). Single layer buckle folding in non-linear materials—ii. comparison between theory and experiment, *J. Struct. Geol.* **14**: 105–120.

Mühlhaus, H.-B., Hobbs, B. E. and Ord, A. (1994). The role of axial constraints on the evolution of folds in single layers, *in* H. J. Siriwardane and M. M. Zaman (eds), *Computer Methods and Advances in Geomechanics*, Vol. 1, A. A. Balkema, Rotterdam, pp. 223–231.

Olver, F. W. J. (1974). *Asymptotics and Special Functions*, Academic Press.

Petzold, L. R. (1982). A description of `DDASSL`: A differential/algebraic system solver, *Technical Report SAND82-8637*, Sandia National Laboratories, Livermore, CA.

Whiting, A. I. M. (1996). *Localized Buckling of an Elastic Strut in a Visco-elastic Medium*, PhD thesis, Imperial College of Science, Technology and Medicine, London.

Whiting, A. I. M. and Hunt, G. W. (1997). Evolution of nonperiodic forms in geological folds, *J. Mathematical Geology* **29**(5): 705–723.

Williams, J. R., Lewis, R. W. and Zienkiewicz, O. C. (1978). A finite-element analysis of the role of initial perturbations in the folding of a single viscous layer, *Tectonophysics* **45**: 187–200.

Zhang, Y., Hobbs, B. E., Ord, A. and Mühlhaus, H.-B. (1996). Computer simulation of single-layer buckling, *J. Struct. Geol.* **18**(5).

Department of Mathematical Sciences, University of Bath, Bath BA2 7AY, United Kingdom
*E-mail address*: C.J.Budd@bath.ac.uk

Department of Mechanical Engineering, University of Bath
*E-mail address*: G.W.Hunt@bath.ac.uk

Departments of Mathematical Sciences and Mechanical Engineering, University of Bath
*E-mail address*: M.A.Peletier@bath.ac.uk